RSC Advances

PAPER

View Article Online
View Journal | View Issue

Cite this: *RSC Adv.*, 2024, **14**, 19271

Au@Ag nanoparticles: an analytical tool to study the effect of tyrosine on dopamine levels

Angel Minj,[a] Sushama Sahu,[b] Lavkesh Kumar Singh Tanwar[a] and Kallol K. Ghosh *[a]

The neurotransmitter dopamine (DA) plays important roles in the human body, including regulatory functions, movement, memory and motivational control. The direct intake of DA is impossible as it cannot cross the blood–brain barrier (BBB) efficiently. Notably, L-tyrosine works as a precursor of DA in the human brain. Herein, we report an analytical method that strongly supports the hypothesis that the intake of tyrosine (Tyr)-rich food enhances DA levels. For this analysis, citrate–coated gold–core silver–shell nanoparticles (Au@Ag NPs) were synthesized. The interaction of DA with the Au@Ag NPs was investigated using multiple spectroscopic techniques, and different thermodynamic parameters were evaluated to assign the binding mechanism. Real sample analysis with Tyr-rich food was also conducted to study the effect of Tyr on DA levels. Analytical studies were performed to verify the outcomes of the present work. The limit of detection of the Au@Ag NPs–DA system for Tyr was found to be 1.64 mM. This study can contribute to development in the fields of medicine and pharmaceuticals, particularly in regard to neuromedicine. One of the major advantages of this investigation is that it will fuel research interest in the supplementation of neurotransmitters and help categorize Tyr as a dietary precursor of dopamine.

Received 11th March 2024
Accepted 31st May 2024

DOI: 10.1039/d4ra01872a

rsc.li/rsc-advances

1. Introduction

Dopamine (DA) is a neurotransmitter found in the human brain and belongs to the catecholamine family.[1–3] Inside the human body, DA is produced in the hypothalamus, ventral tegmental area and substantia nigra of the brain.[2,3] DA plays a vital role in the human body as it is related to the renal, cardiovascular, hormonal and central nervous systems.[3] It is also one of the major modulators of the functioning of the human body. High dopamine levels induce cardiotoxicity, leading to hypertension, heart failure, *etc.*,[2–4] whereas low levels can cause major neurological diseases, such as parkinson's disease, schizophrenia and alzheimer's disease.[5] DA also holds social importance as it plays an important role with respect to human behaviour and habits.[6] The direct precursors of DA are L-DOPA, *p*-tyramine and *m*-tyramine, whereas the administrative precursor of these three is L-tyrosine (Tyr).[7] Other than these functions, DA acts as a precursor of epinephrine and norepinephrine.[7,8]

Tyr is a non-essential aromatic amino acid, which is synthesized from phenylalanine in the brain.[9–11] Tyr is a primary constituent of proteins and is important for maintaining the nitrogen level in the human body.[10] It is minimally present in fruits and vegetables and hence can be balanced by the intake of wheat, meat and dairy products. Tyr has a crucial influence on neurotransmitters, hormones, pigments and some proteins.[11] Importantly, Tyr is the biochemical precursor of the neurotransmitter DA, epinephrine and norepinephrine.[12] DA is primarily produced from Tyr *via* the tyrosine–hydroxylase enzymatic reaction, which forms L-DOPA as the intermediate.[13] Thus, Tyr can be potentially applied as nutritional and pharmaceutical supplementation to maintain DA levels.[14] It is necessary to quantify the amounts of DA and Tyr in the body and food samples as they should be present in the human body in specific quantities.[15] In this context, nanoparticles (NPs) have been successfully used to quantify the amount of Tyr and DA using analytical approaches. This has helped researchers to look ahead of conventional methods, such as HPLC, gas chromatography, and chemiluminescence, for the detection of DA and Tyr.[16,17] Tyr along with NPs has successfully been explored as a sensor, inhibitor, adsorbent and drug carrier.[17] Previously, Tyr-based AgNPs have shown great antibacterial activity and biocompatibility with mammalian epithelial cells.[18] While DA cannot cross the blood–brain barrier (BBB),[19] NPs have made this possible by loading and delivering it to the targeted site.[20] Tyr-functionalised NPs have also been used for targeted drug delivery in the human body.[21]

Besides monometallic nanoparticles, bimetallic nanoparticles (BMNPs) have attained great attention as they exhibit intriguing optical, electrical, and magnetic properties due to the synergistic effect of the constituent metals.[21] Their synergistic effect results in improved properties of BMNPs compared with

[a]*School of Studies in Chemistry, Pt. Ravishankar Shukla University, Raipur-492010, Chhattisgarh, India. E-mail: kallolkghosh@gmaill.com; Tel: +91-94252 16204*
[b]*Govt. Narayanrao Meghawale Girls College, Dhamtari, Chhattisgarh, India*

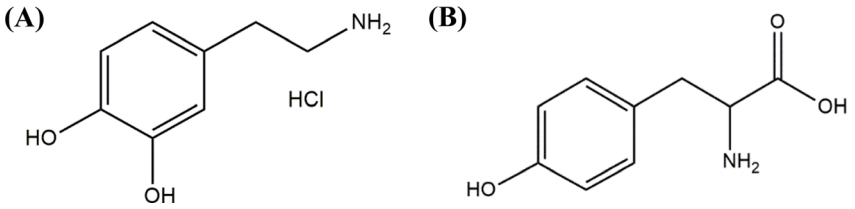

Scheme 1 Chemical structures of (A) dopamine hydrochloride and (B) L-tyrosine.

monometallic NPs. They can be synthesized by the combination of different metals, such as Ag–Au, Ag–Cu, Pt–Ag, Au–Pd, and Au–Pt.[22–25] The presence of plasmonic properties along with noble metals in BMNPs diversifies their application scope.[22,25] BMNPs help in tuning the surface plasmon resonance (SPR) and enhance the dispersion and stability of particles.[22] This shows their advantages in significant domains, such as sensing, catalysis, carriers, imaging and diagnosis.[23,24]

In this investigation, the interactional study of DA with gold–core silver–shell nanoparticles (Au@Ag NPs) was carried out using different spectroscopic techniques, including UV-visible spectroscopy, transmission electron microscopy (TEM), energy dispersive X-ray diffraction (EDX), and Fourier transform infrared (FTIR) and X-ray photoelectron spectroscopy (XPS). The concept that L-Tyr is the precursor of DA in the human brain and regulates the DA level is not experimentally proven and remains largely hypothetical. Therefore, this investigation was carried out to justify this hypothesis using various thermodynamic and analytical approaches. Further, these NPs were applied as an analytical tool for real sample analysis to justify that tyrosine-rich food directly affects the regulation of DA in the human body and serves as the dietary precursor of DA. This work provides a holistic approach to understanding DA regulation. Through this analysis, it will be possible to comprehend how Tyr activates and regulates the DA level. The proposed method is cost-effective, sensitive and easy to handle compared with the traditional analytical methods employed to study such interactions.

The chemical structures of dopamine hydrochloride and L-tyrosine are given in Scheme 1.

2. Experimental section

2.1. Chemicals and reagents

All the chemicals used in this investigation were of analytical grade and were used without further purification. Silver nitrate ($AgNO_3$, ≥99.0%), auric chloride ($HAuCl_4$, 99.9%), sodium borohydride ($NaBH_4$, ≥98.0%), tri-sodium citrate ($Na_3C_6H_5O_7$, ≥99%), dopamine hydrochloride ($C_8H_{11}NO_2$, 98%) and L-tyrosine ($C_9H_{11}NO_3$, ≥98%) were purchased from Sigma-Aldrich Pvt. Ltd. All the solutions were prepared in double-distilled water.

2.2. Instrumentation

The absorption spectra of Au@Ag NPs in interaction with different samples were recorded using a UV-visible spectrophotometer (Cary 60, Agilent Technologies) in the range of 200–800 nm. A Nicolet iS10 Fourier transform infrared (FT-IR) spectrometer, (Thermo Fisher) was used for the analysis of different functional groups. The transmittance spectra were recorded based on 64 scans with a 4 cm^{-1} resolution between 500 to 4000 cm^{-1} using potassium bromide (KBr) matrixes. Dynamic light scattering (DLS) (Malvern Panalytical) was used for measuring the zeta potentials of the sample solutions. High-resolution transmission electron microscopy (HR-TEM) was used to determine the size and shape of the Au@Ag NPs using a Tecnai G2, F30 at an accelerating voltage of 300 kV, and CM 200 operating at an accelerating voltage of 200 kV was used for the Au and Ag monometallic NPs. To investigate the elemental composition of the surface and different layers of the materials, X-ray photoelectron spectroscopy (XPS) was performed using a Nexsa Base (ThermoFisher Scientific) at 1.00 eV.

2.3. Synthesis of nanoparticles

2.3.1 Synthesis of gold nanoparticles. The traditional Turkevich method was used for the synthesis of AuNPs with slight modifications.[26,27] First, $HAuCl_4$ salt (0.002 M) was dissolved in 100 mL double-distilled water and stirred for 15 minutes in a chilled water bath, followed by the dropwise addition of $NaBH_4$ (0.01 M) till the appearance of a wine-red colour. The mixture was stirred for another 15 minutes, after which 1.0 mL of a citrate solution (0.03 M) was added and stirred continuously. The appearance of wine-red colour indicated the formation of citrate–capped AuNPs.

2.3.2 Synthesis of silver nanoparticles. The AgNPs were synthesized using a chemical reduction method.[28,29] For this, $NaBH_4$ (0.01 M) was dissolved in 100 mL distilled water and stirred in a cold water bath for 10 minutes. After the complete dissolution of $NaBH_4$, 1.0 mL of citrate (0.03 M) was added dropwise under stirring. Further, $AgNO_3$ (0.01 M) was mixed drop by drop till the solution turned yellow, which indicated the synthesis of AgNPs.

2.3.3 Synthesis of gold@ silver core–shell nanoparticles (Au@Ag NPs). The synthesis of Au@Ag NPs was carried out with slight modifications to the reported methods.[30,31] Monometallic Au and Ag NPs were mixed at an equimolar ratio and stirred for 15 minutes. The appearance of an orange-red solution indicated the successful synthesis of Au@Ag NPs. The different colours of the monometallic and core–shell NPs are shown in Scheme 2.

2.4. Interaction of Au@Ag NPs with dopamine

The interactional study of DA with Au@Ag NPs was performed using multiple spectroscopic techniques. For this, different amounts of dopamine hydrochloride (1.0 mM; source of

Scheme 2 Red, yellow and orange represent Au, Ag and Au@Ag NPs (core–shell), respectively.

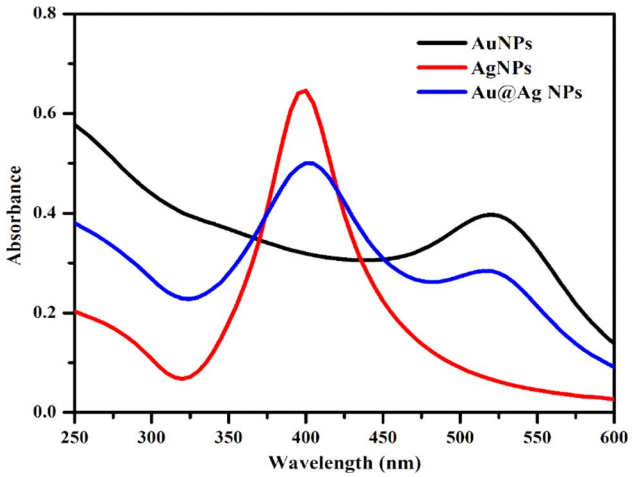

Fig. 1 UV-visible spectra of AgNPs, AuNPs and Au@Ag NPs.

dopamine) were added to the Au@Ag NPs sample. Their interaction was studied by UV-visible and FT-IR spectroscopies. The interaction was optimized by studying the effects of environmental conditions, such as temperature, pH and various interfering substances.

2.5. Sample collection and pre-treatment

A variety of food samples were collected as Tyr sources from the local Raipur grocery store. For the analysis, 3.0 g of each sample was dry-crushed using a mortar-pestle and diluted in 5.0 mL of double-distilled water. The prepared sample solutions were further diluted using 1.0 mL of the concentrated solution to a final volume of 3 mL. After this, each sample was filtered three times using Whatman filter paper no. 42 to remove sedimental impurities. The filtrates were used as the Tyr-rich samples to study their effects on DA using Au@Ag NPs.

3. Results and discussion

3.1. Physicochemical characterization of the Au@Ag NPs

Various techniques were adapted to understand the physicochemical nature of the NPs. UV-visible spectroscopy was used as the primary technique to confirm the formation of the metallic NPs. Intense absorption peaks of Au and Ag NPs were observed at 520 and 410 nm, respectively, due to surface plasmon resonance (SPR), indicating the successful synthesis of these NPs. Meanwhile, the appearance of two intense distinguishable peaks at 520 and 410 nm indicated the presence of both NPs in the solution of Au@Ag NPs (Fig. 1). Analysis by HR-TEM was done to find the particle size distribution. The HR-TEM images of Au, Ag and Au@Ag NPs revealed their spherical shape with average sizes of 13, 21 and 29 nm, respectively. This indicates that the sizes of the monometallic NPs were comparatively larger and randomly distributed, and the uniform dispersion of the Au@Ag NPs suggests that it was not a physical mixture of individual NPs and the desired core–shell NPs were formed (Fig. 2). The elemental mappings and chemical compositions of the samples were investigated with EDX, which suggested the presence of both metal ions within the Au@Ag NPs as the characteristic intense peaks of Ag and Au appeared, as shown in Fig. 3. From these results, it can be concluded that the Au@Ag NPs existed in the core–shell form. The intense peak of Ag represents the shell surrounding the dense Au core, as seen in the summarized peak with reference to Ag, thus verifying the formation of gold–silver–based core–shell NPs, *i.e.*, Au@Ag NPs.

An XPS analysis was carried out to examine the composition and valence of Au@Ag NPs in the presence and absence of DA. Fig. 4(A and B) show the respective spectra of Au@Ag NPs, in which the peaks at around 1100, 650 and 290 eV display the presence of Na, O and C, respectively. They originate from the capping molecule (tri-sodium citrate) used during the synthesis of NPs. The signals at 400 and 375 eV can be attributed to the 1s and 3d orbitals of N and Ag, respectively, while the signals observed at around 100 and 200 eV represent the 4f and 2p shells of Au and Cl, due to the respective precursors used for the synthesis of silver and gold NPs. Similar results were observed for Au@Ag NPs with dopamine.

The binding energy peaks demonstrate that Au comprised the core and Ag comprised the shell of the Au@Ag NPs as Au has a lower binding energy than Ag. In XPS, which is a surface-sensitive technique that measures the kinetic energy, the binding energy of Ag (shell) was comparatively higher than that of Au (core). The higher binding energy peak corresponds with the first surface interaction, followed by that on the inner layer. The peak intensity of surface material helps us to assess the content of a particular element on the surface. The obtained results indicated a layer of Ag on the surface, and compared with Ag, Au had a peak of lower intensity and binding energy, which suggests that Au was in the inner layer of the NPs. Both monometallic counterparts Ag and Au were present in the zero-valent state. The XPS data of Au@Ag NPs before and after the addition of DA were compared (Tables 1 and 2). The interaction of DA with the surface layer is expected to occur through hydrogen bonding between the nitrogen and oxygen present in the DA and citrate molecules, respectively.

FTIR was used as an analytical tool to ensure the successful capping and bonding between the molecules. The characteristic IR band that appeared at 1507 cm^{-1} corresponded to the C–H bending of alkane and the strong C=O stretching band observed at 1698 cm^{-1} indicated the presence of a citrate group.

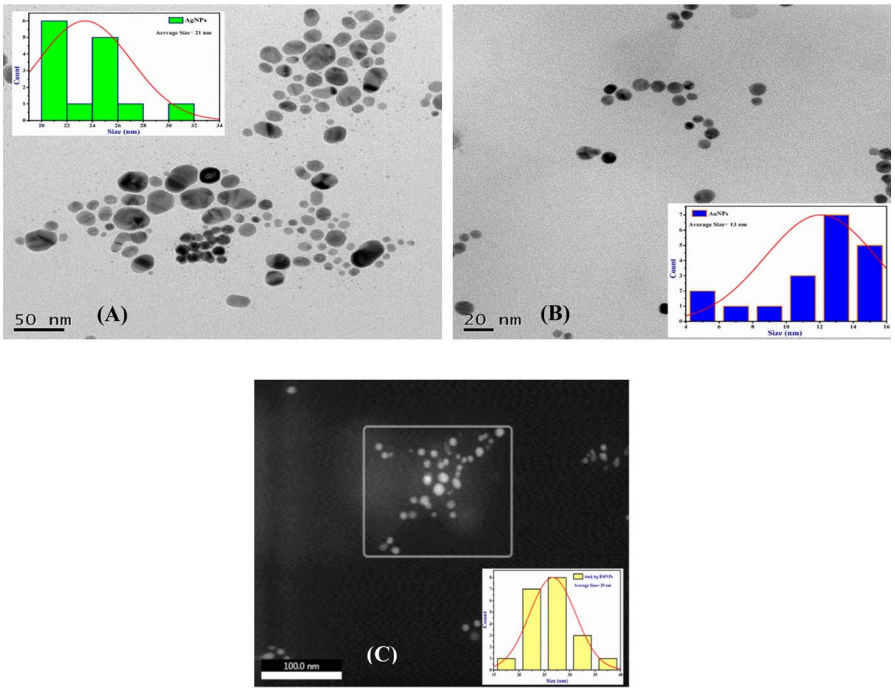

Fig. 2 HR-TEM images of (A) AgNPs, (B) AuNPs and (C) Au@Ag NPs.

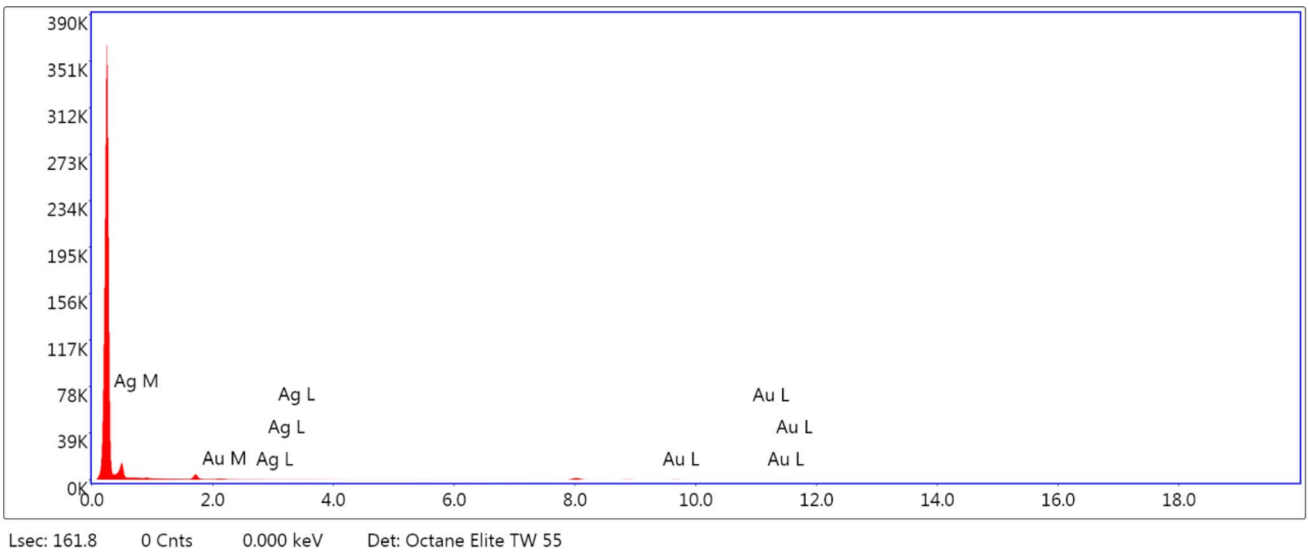

Fig. 3 EDX spectra of Au@Ag NPs.

The surface modification of Au@Ag NPs with tri-sodium citrate was confirmed by the band of O–H stretching at around 3500 cm^{-1}, as seen in Fig. 5. The FTIR spectrum of Au@Ag NPs had similar peaks as the precursors, and the formation of the core–shell structure was confirmed based on previous reports.[30,32,33] The characteristic peak of the phenolic O–H stretching of DA was found at around 3550 cm^{-1} and that of N–H bending of amine appeared at around 1600 cm^{-1}.[34,35] The stretching bands at around 3400 cm^{-1} and 1500 cm^{-1} could be assigned to the amine (N–H) and aromatic C=C of DA (Fig. 5). The peaks at 3550 cm^{-1} and 1507 cm^{-1} increased after the addition of DA compared with those of the pure Au@Ag NPs. An efficient increase in signal intensity at 3740 cm^{-1} indicated the presence of free –OH groups, confirming the presence of DA on the surface of the NPs (Fig. 5). The changes in the intensity of the peaks indicated the successful binding of DA with Au@Ag NPs.

3.2. Interactional mechanism of Au@Ag NPs with dopamine

The Au@Ag NPs formulated from monometallic Au and Ag NPs were investigated for their interaction with DA as they show outstanding catalytic activity compared with the monometallic

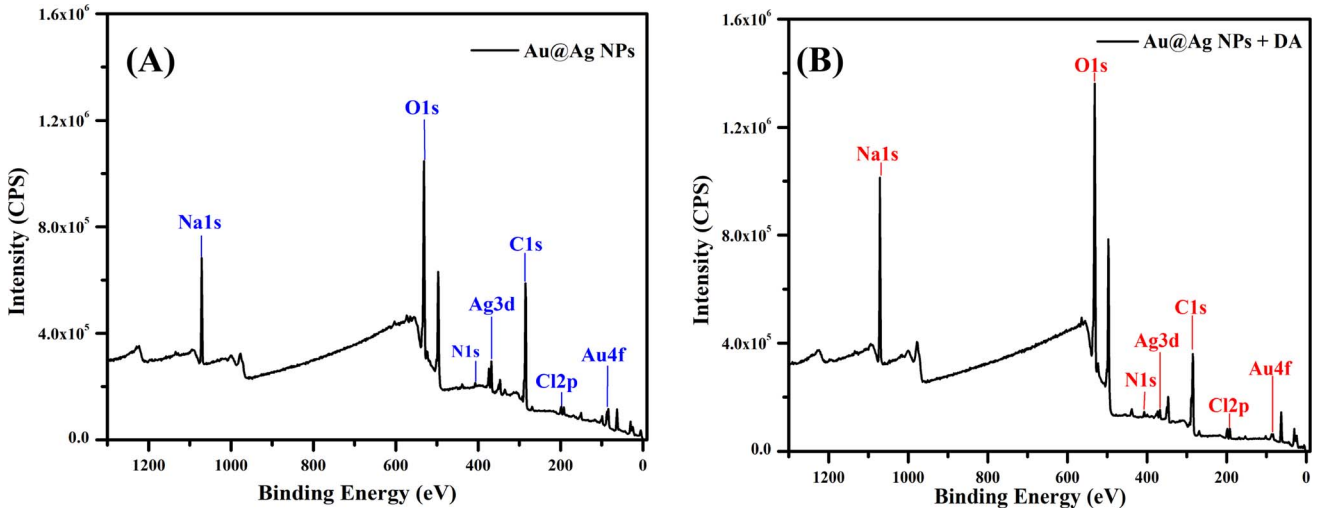

Fig. 4 XPS spectra of (A) Au@Ag NPs and (B) Au@Ag NPs with dopamine.

Table 1 XPS Spectra of Au@Ag NPs

Elements	Peak (BE)	Area (*P*) CPS	Atomic%
C 1s	284.66	7758.95	55.34
O 1s	531.37	14 658.35	43.24
Ag 3d	367.71	2444.52	0.83
Au 4f	83.57	1910.35	0.58

Table 2 XPS Spectra of Au@Ag NPs–DA

Elements	Peak (BE)	Area (*P*) CPS	Atomic%
C 1s	284.69	6594.82	28.82
O 1s	531.32	19 968.28	36.09
Ag 3d	367.48	857.86	0.18
Au 4f	83.36	753.04	0.14

NPs. During the synthesis of the NPs, the BH_4^- anion reduces the metal ions into zero valent metal by getting adsorbed on the surface of metal ions. Here, the citrate molecule is used as the capping agent that jackets the metal through chemisorption. This provides particle colloidal stability by inducing a negative surface charge on the metal and results in electrostatic repulsion.[36] This arises due to the presence of electrostatic charge on the particle surface and steric stabilization, which prevents the particles from aggregation.[37] The citrate molecule is also used to prevent the growth of particles following the Ostwald ripening phenomenon.[34] Here, the central carboxyl group of citrate ion binds with the positively charged metal atom by the donor–acceptor phenomenon, in which Ag and Au act as soft Lewis acids, while citrate behaves as a soft Lewis base.[33,38,39]

In this work, the Au@Ag NPs were synthesized by physically mixing the colloidal dispersion of monometallic Ag and Au NPs.[40] The expected mechanism of their fabrication is through self-organisation (Scheme 3). Due to their larger size, the AgNPs tend to adsorb on the surface of the smaller-sized AuNPs with a greater surface area. The AgNPs tend to form a layer, which acts as a shell on the surface of the AuNPs, by the phenomenon of mutual diffusion. The surface energy of Ag (1.25 J m^{-2}) is comparatively lesser than Au (1.50 J m^{-2}), which favours the surface enrichment of AgNPs.[40,41] Also, the cohesive energy of Au (3.81 eV per atom) is remarkably greater than that of Ag (2.95 eV per atom).[40,42,43] The greater cohesive energy causes better metal–metal bond strength *i.e.*, Au–Au > Ag–Ag favours the formation of an Au-enriched core.[40]

With the addition of DA, it binds with the remaining binding sites *via* citrate by the adsorption phenomenon. The interaction of the NPs with DA through hydrogen bonding, hydrophilic/hydrophobic and van der Waal interactions has also been observed. The possible interaction mechanism is depicted in Scheme 4, which is strongly supported by the UV-visible absorbance and DLS zeta potential measurements (Fig. 6 and Table 3). The characteristic absorption peak at 280 nm and the increase in the zeta potential of the Au@Ag NPs from −29.37 mV to −21.39 mV after the addition of DA confirms the successful interaction of Au@Ag NPs with DA. The change in SPR with respect to the Au peak was obvious with the addition of DA. The reason behind such changes can be the conjugation of different factors associated with the bimetallic system. It can majorly occur due to the thin shell over the Au core due to which the plasmonic field can easily penetrate. The plasmonic fields of the core and shell tend to couple, potentially causing the changes in core SPR to have a greater impact than the changes in the shell.[44]

Further, to study the effect of Tyr on DA, the concentration effect was also studied. A hyperchromic shift in the absorption band was observed, indicating that Tyr binds with DA in this system and influences the fate of DA (Fig. 10A). The absorption spectra tended to increase linearly with increasing Tyr concentration.

3.3. Chemistry behind DA enhancement through Tyr supplementation

In order to study the possible effect of Tyr on the DA signal, we examined the absorptivity of DA on Au@Ag NPs before and after

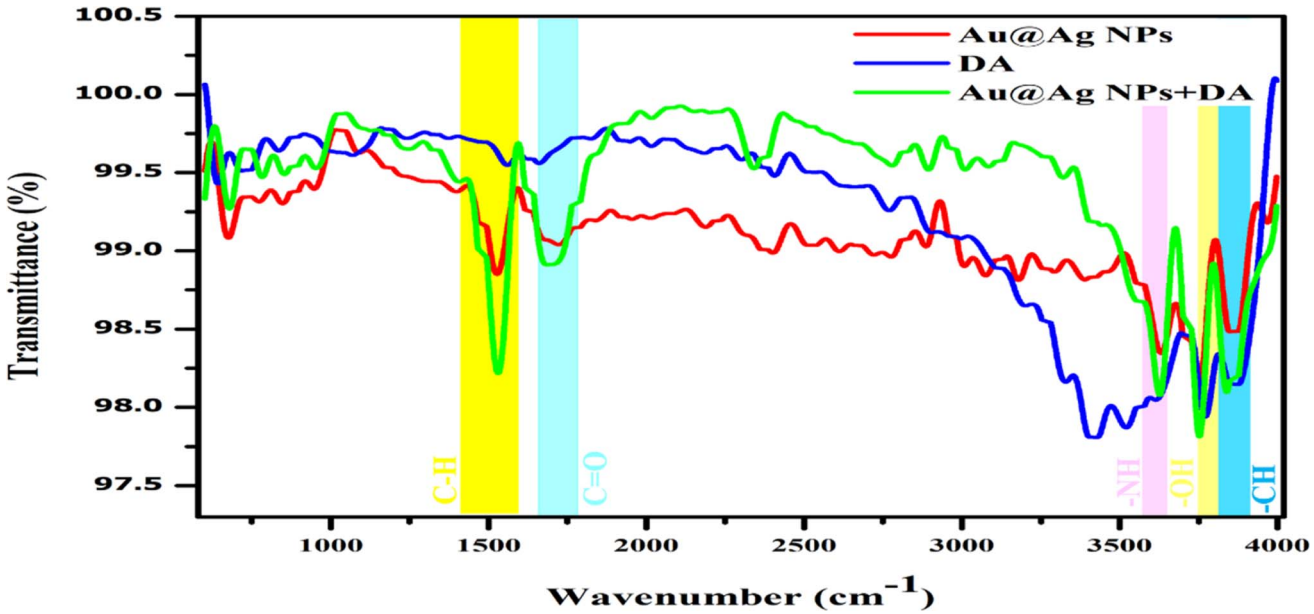

Fig. 5 FTIR spectra of Au@AgNPs, dopamine and Au@Ag NPs after the addition of dopamine.

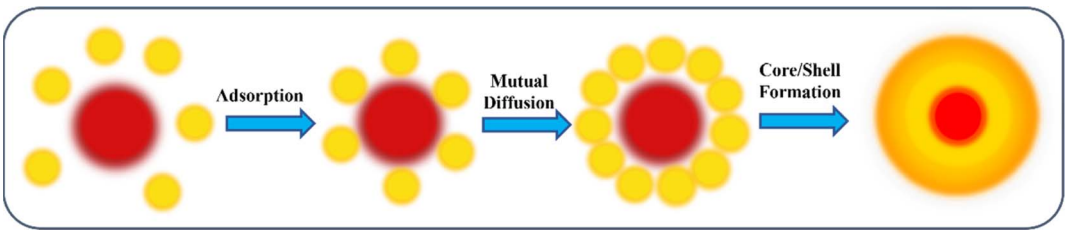

Scheme 3 Formation mechanism of Au@Ag NPs from monometallic AgNPs and AuNPs.

the addition of Tyr. Here, Tyr enhanced the activity of DA, as confirmed by the hypochromic (blue) shift of the signal, which suggests the formation of a more stable complex.

According to previous reports, L-tyrosine is converted into L-DOPA and then dopamine.[13] This process is categorized as biotransformation *i.e.*, a single amino acid L-tyrosine is

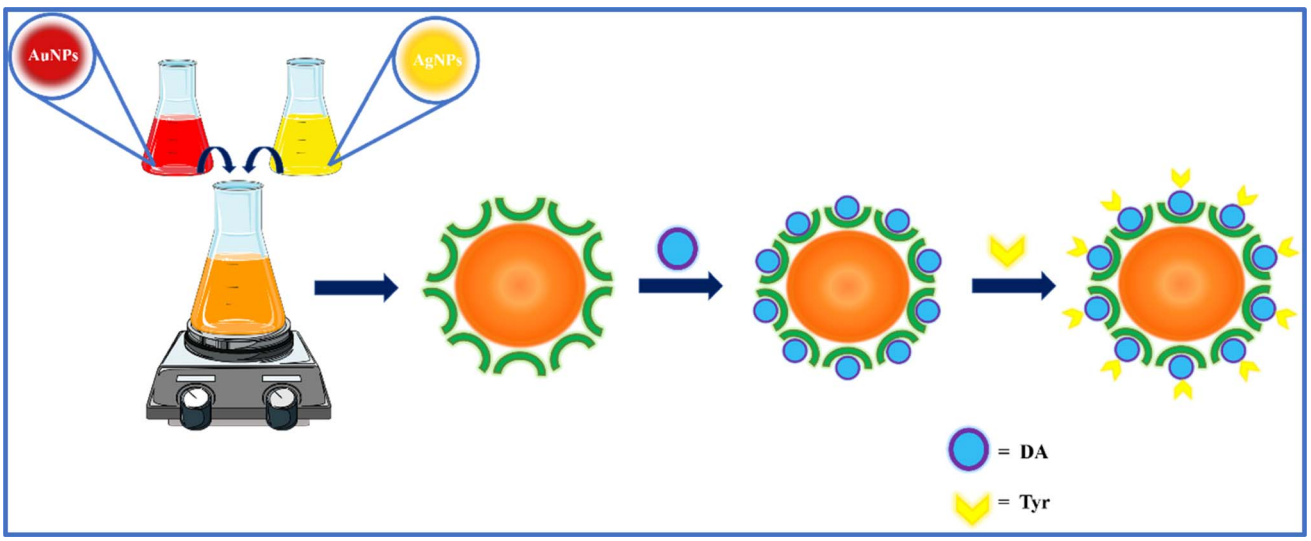

Scheme 4 Interaction mechanism of Au@Ag NPs with DA and Tyr.

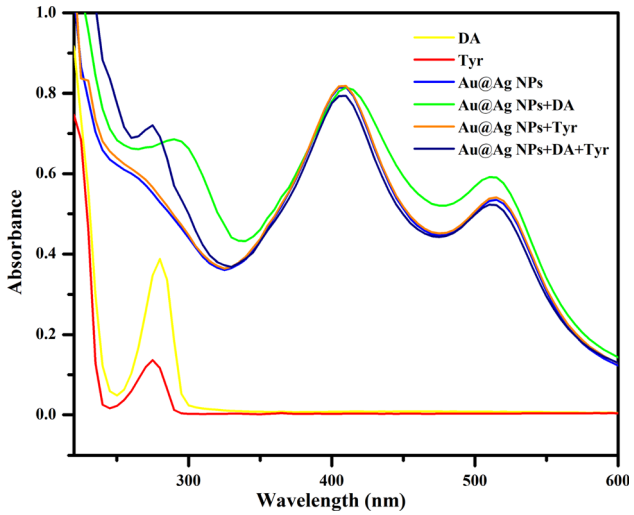

Fig. 6 UV-visible spectra of pure DA, Tyr, Au@AgNPs, Au@AgNPs–DA, Au@AgNPs–Tyr and Au@AgNPs–DA–Tyr.

Table 3 Zeta potentials (ζ) of Au@Ag NPs, DA and Au@Ag NPs with DA

S. no.	Sample	Zeta potential (ζ) (mV)
1	DA	17.17 ± 0.07
2	Au@Ag NPs	−29.37 ± 0.03
3	Au@Ag NPs + DA	−21.39 ± 0.06

hydroxylated into L-DOPA by tyrosinase in the pathway of DA biosynthesis and then converted into dopamine.[47] The major difference between L-DOPA and dopamine is that L-DOPA crosses the protective blood–brain barrier, whereas dopamine cannot.[19] The major common precursor of L-DOPA and DA is Tyr.[7] Hence, Tyr plays a key role in increasing the concentration of dopamine for the treatment of various diseases, including Parkinson's disease, dopamine-responsive dystonia, Parkinsonism and Parkinson-plus syndrome.[5]

These different forms can be distinguished through FTIR analysis, but the analytical process is yet to be established and can be a subject of future research. The present findings explain the DA enhancement effect of Tyr. Interestingly, there was a notable enhancement in the absorptivity of dopamine with the formation of a highly stable complex, as shown in Scheme 5.

3.4. Interference study of Au@Ag NPs using other chemical substances

To validate the selectivity of the prepared Au@Ag NPs towards DA, the interference study has been performed with different chemical substances (Fig. 7A). For this purpose, various biomolecules (valine, glycine, cysteine, leucine) and ions (Br^{-}, I^{-}, Li^{+}, Mn^{+2}, Cu^{+2}, Ni^{+2}, Pb^{+2}, Cd^{+2}) were tested at a 0.01 M concentration under the same reaction condition. It was seen that no other molecules interfered with the interaction of DA and the bimetallic NPs. Only DA gave absorption spectra in the characteristic range, whereas no other molecule caused a noticeable alteration in the absorption spectrum in this range with Au@Ag NPs.

Further, the selectivity study of DA towards Tyr was also performed by assaying different amino acids in the DA-interacted Au@Ag NPs system under the same reaction condition (Fig. 7B). There was no measurable change for the other amino acids, such as cysteine, valine, glycine and leucine. A notable blue shift and enhancement in absorption intensity was seen only in the presence of Tyr.

The result suggested that our system has better selectivity towards the enhancement study of DA through Tyr under the proposed reaction condition.

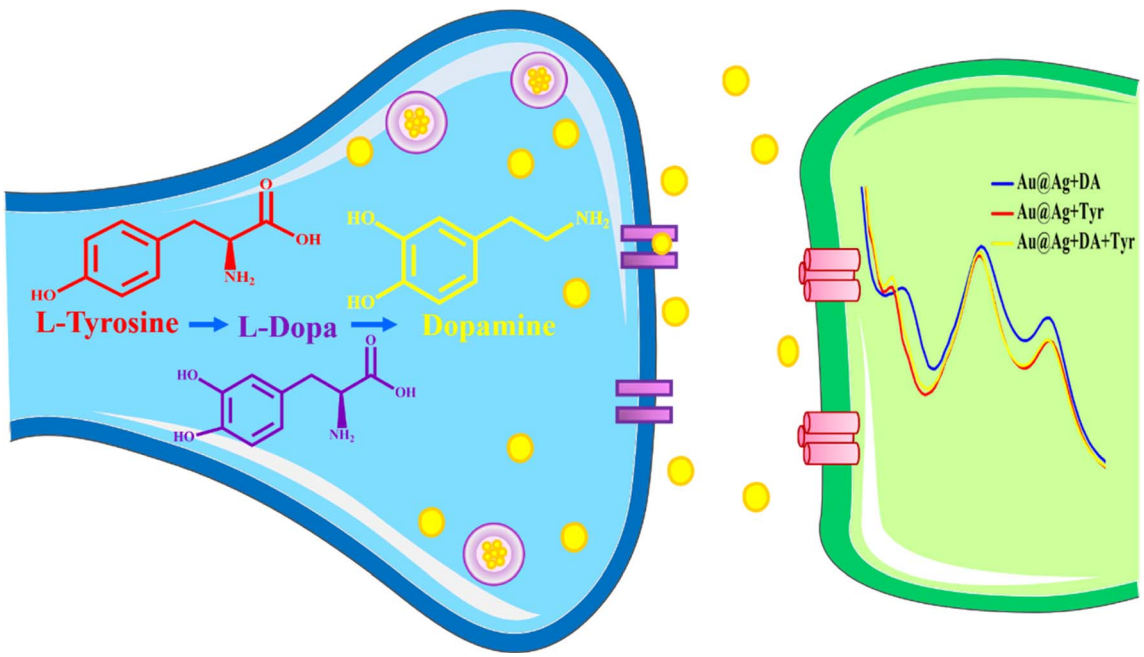

Scheme 5 Dopamine metabolism pathway.

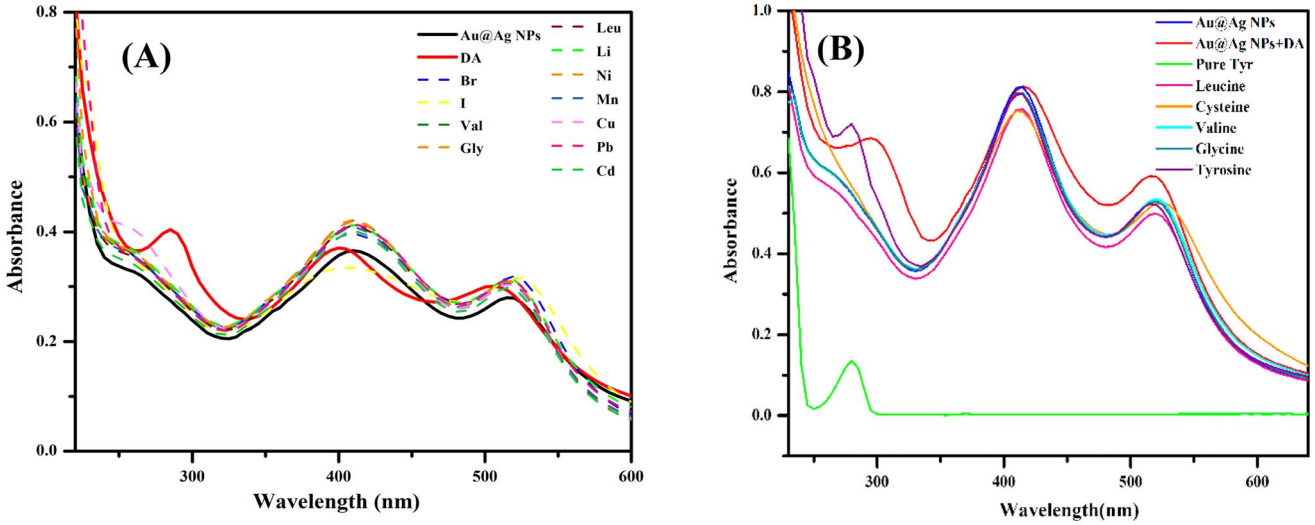

Fig. 7 UV-visible spectra showing the (A) effect of different interfering substances on the Au@Ag NPs–DA system and (B) effect of different biomolecules on the interaction of the Au@Ag NPs–DA system with Tyr.

3.5. Optimization of Au@Ag NPs

The proposed system was optimized by studying the effects of time and pH on the interaction of DA with Au@Ag NPs (Fig. 8). Fig. 8A shows the absorption spectra of the interaction of Au@Ag NPs with DA in the pH range of 4 to 12. There was no significant change in the absorption spectra, verifying that the interaction of DA did not depend on the pH.

Moreover, the stability of the Au@Ag NPs was investigated over time by measuring the absorption intensity (Fig. 8B). After the addition of DA to Au@Ag NPs, the stability of sample solutions was checked every 5 minutes for half an hour and then on days 5, 10, and 45. The system has also been performed with Tyr to perform an enhancement study and the system reported the same result as the previous one. Thus, the system was found to be feasible for a long time with Au@Ag NPs. Hence, the proposed system was found to be highly stable and facile towards the interaction with DA.

3.6. Thermodynamic evaluation and nature of binding

To understand the binding phenomena and stability of the system, we studied the binding constant and different thermodynamic parameters using UV-visible spectrophotometry. The study was conducted at three different temperatures, Fig. 9(A–C) show the UV-visible spectra at temperatures of 283, 298 and 313 K, respectively. Different thermodynamic parameters, including Gibbs free energy (ΔG), enthalpy (ΔH) and entropy (ΔS), can give an idea regarding the binding nature of the analyte molecule and the driving forces responsible for the interaction. The negative ΔG and ΔH values indicate the spontaneous and exothermic nature of the reaction medium, respectively, as a more negative value shows greater thermodynamic stability of the system. The values of ΔS, ΔH and ΔG indicate the forces associated with an interaction.[45,47] The binding phenomenon can occur through hydrogen bonding, hydrophilic/hydrophobic interactions, and van der Waals and electrostatic forces. The values of ΔH and ΔS were found to be negative and positive, respectively; thus van-der Waals interaction and hydrogen bonding will be the predominant modes of interaction.[47]

Different thermodynamic parameters associated with the reaction were calculated using the van't Hoff expression (eqn (1)) and Gibbs free energy formula (eqn (2)), while the binding constant was calculated using eqn (3):

$$\ln K_a = -\frac{\Delta H}{\Delta T} + \frac{\Delta S}{\Delta R} \quad (1)$$

$$\Delta G = \Delta H - T\Delta S \quad (2)$$

$$\frac{1}{A - A_o} = \frac{1}{\{K_a(A_{max} - A_o)(c)\}} + \frac{1}{\{A_{max} - A_o\}} \quad (3)$$

where K_a is the associative binding constant at temperature T, and R is the gas constant (8.314 J mol^{-1} K^{-1}). $\Delta H < 0$ indicates that the system releases energy, and $\Delta S > 0$ indicates an entropy-driven process. These parameters were calculated from the linear fitting plot, and the resultant values are summarized in Table 4. The increase in values of the binding constant with temperature indicated the formation of strong bonds between the Au@Ag NPs–DA system. An increase in the absorption band was observed due to the increase in stability due to the formation of strong bonds. The binding constant was calculated using the Benesi Hildebrand eqn (3).[46,47] The entire absorption spectrum underwent a hyperchromic shift with the gradual addition of DA to the Au@Ag NPs solution (Fig. 9), indicating the possibility of ground–state complex formation.

3.7. Applicability of the proposed methodology in real samples

The food consumed by humans has a major impact on the functioning of the human body. Along with micronutrients, various macronutrients are also required in specific quantities.

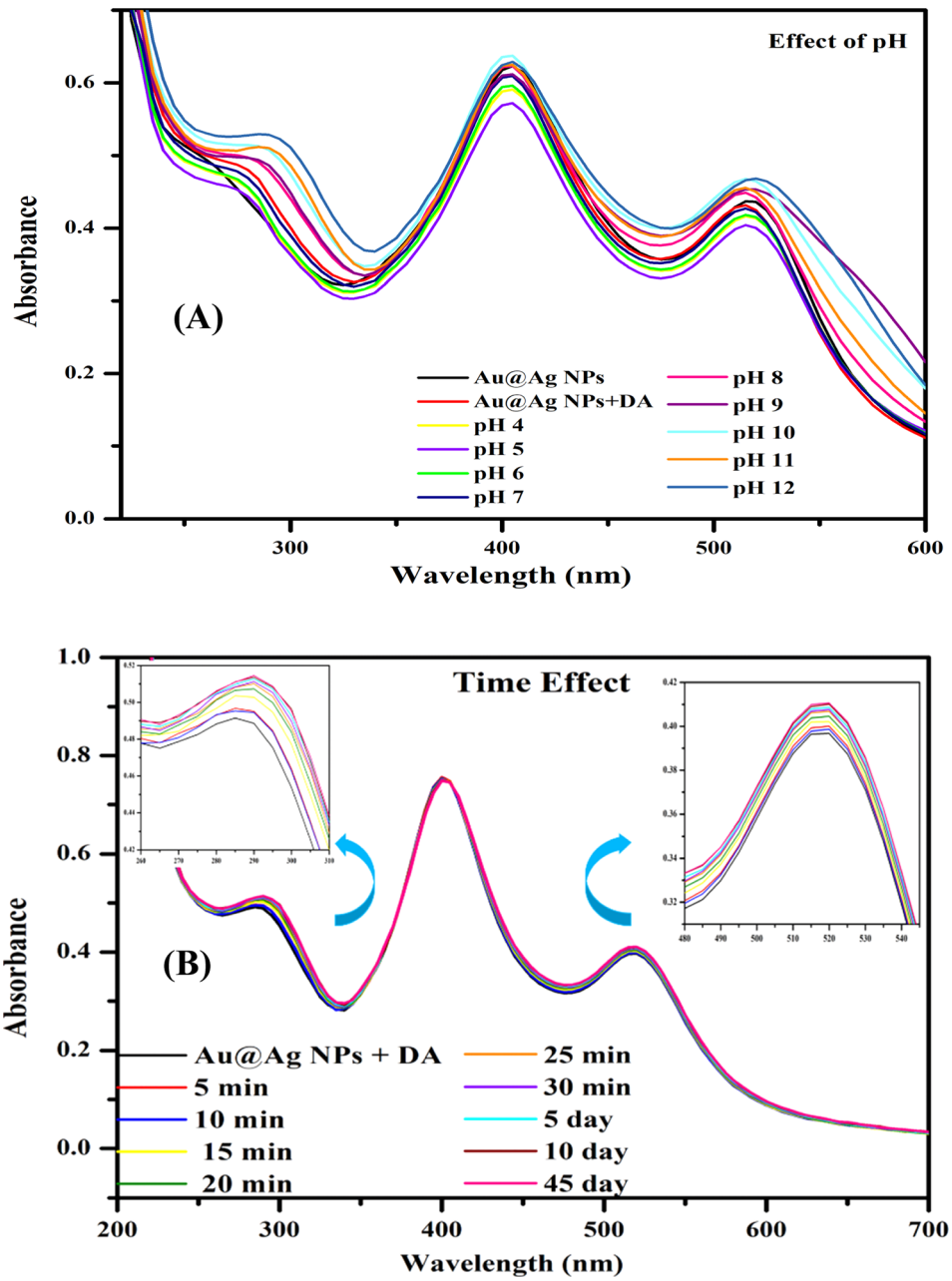

Fig. 8 Optimization of the Au@Ag NPs–DA system: (A) different pH values and (B) time periods.

Tyr is a class of amino acids, a macronutrient that is also the metabolic precursor of DA.[48] A precise amount of Tyr is therefore essential for humans as it is also responsible for the metabolism of DA. Analytically, we have demonstrated that the Tyr is able to modulate DA, which can be upregulated under disease conditions, as well as aid in their prevention. In previous research works, it has been demonstrated that Tyr-based drugs are used in early clinical treatment to reverse DA toxicity in human neurons.[49] To counter the different side effects caused by drugs, maintaining the Tyr level through dietary intake can be a healthy way. Au@Ag NPs interacting with DA were used as a platform to study the effect of dietary Tyr supplementation on DA. In this analysis, various samples rich in Tyr led to different changes in the absorption signature peak at 290 nm. There was an enhancement in the absorption intensity of Au@Ag NPs–DA with increasing Tyr concentration from 0 to 30 mM (Fig. 10A). The effective concentration of Tyr in the food samples was then calculated using the linear least square equation $y = 0.67691 + 0.00118x$ obtained from the linear fitting plot (Table 5) (Fig. 10B).

3.8. Analytical evaluation of the proposed system

The standard calibration curve of Tyr was constructed to determine the concentration of Tyr in real samples using the Au@Ag NPs–DA system. This was performed by adding different amounts of Tyr (0.01 M) (100–1000 μL) to 2 mL of the Au@Ag NPs–DA solution and diluting it to 3 mL with distilled water.

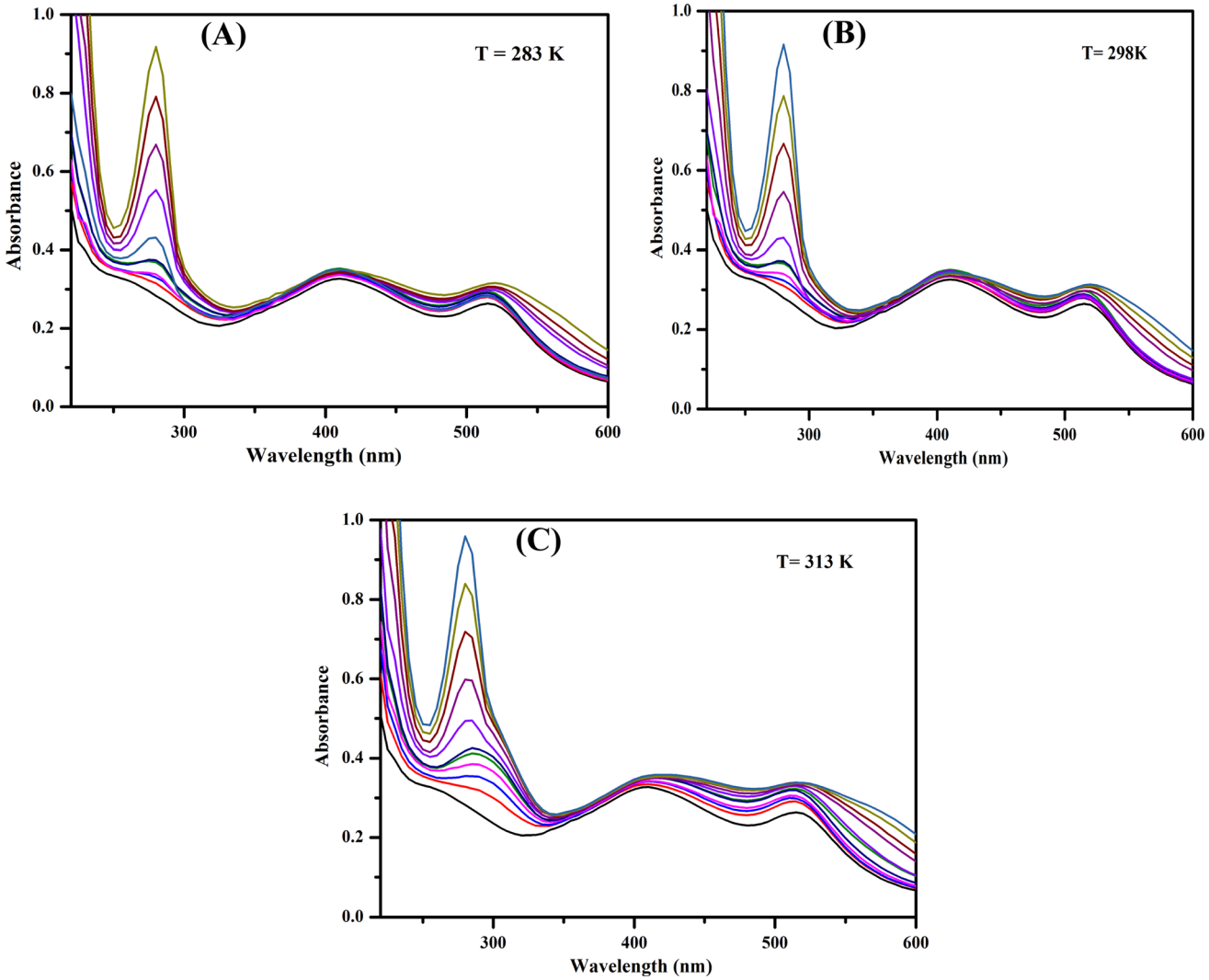

Fig. 9 (A–C) UV-visible spectra of Au@Ag NPs in the presence of dopamine at temperatures of 283, 298 and 313 K.

Table 4 Calculated binding constants and different thermodynamic parameters of the Au@Ag NPs–DA system

Temperature (K)	$K_a \times 10^4$	ΔH (kJ mol^{-1})	ΔS (J mol^{-1} K^{-1})	ΔG (kJ mol^{-1})
283	1.31 ± 0.02	−2.35 ± 0.01	70.52 ± 0.04	−22.31 ± 0.07
298	1.51 ± 0.04	−2.48 ± 0.05	71.70 ± 0.02	−23.84 ± 0.03
313	1.58 ± 0.07	−2.60 ± 0.04	72.08 ± 0.08	−25.16 ± 0.02

The absorption intensity at 274 nm was recorded at different concentrations of Tyr. The absorption intensity tended to increase with increasing concentration of Tyr. Thus, a straight line was observed with a correlation coefficient (R^2) of 0.918. The limit of detection (LOD) was calculated by the 3σ method, and the value was found to be 1.64 mM (standard error ± 0.0012). Further, the relative standard deviation percentage (RSD%) was calculated from five successive analyses under the same reaction condition. An RSD value of 0.993% was noted, indicating appreciable precision of the proposed methodology.

3.9. Comparative study

This investigation reports the development of an analytical platform with the help of nanotechnology. Novel bimetallic NPs using Au and Ag, *i.e.* Au@Ag NPs, have been considered to design a powerful technique. The system was allowed to interact with DA and their interactional mechanism was studied with the help of different analytical instruments. The developed system was further applied to study the modulatory effect of Tyr on DA. The proposed work is considered one of a kind compared with other reported works on DA and its modulation.

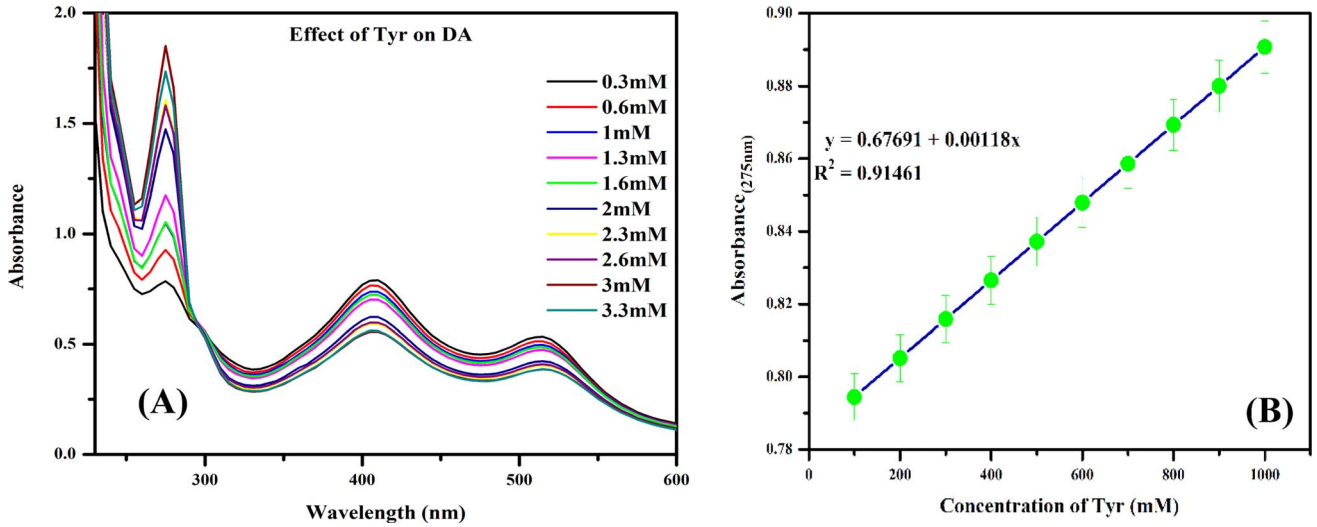

Fig. 10 (A) Effect of Tyr concentration on the Au@Ag NPs–DA system and (B) standard calibration curve for Tyr with respect to Au@Ag NPs–DA sensor.

Table 5 Effective concentrations of Tyr in real samples calculated using Au@Ag NPs–DA as the sensing platform

S. no	Sample	Effective concentration (mg mL^{-1})	RSD%
1	Milk	41.69	0.930 ± 0.02
2	Almonds	94.23	1.26 ± 0.05
3	Beans	49.63	1.39 ± 0.03
4	Melons	55.08	2.99 ± 0.07
5	Pumpkin	23.68	1.01 ± 0.08
6	Sesame	25.84	2.79 ± 0.05

The simple, selective, sensitive and single-step method makes the investigation advantageous. In the literature, NPs have been used to detect DA through Tyr modification or *vice versa*. A variety of NP-based approaches have been explored for the determination of DA and Tyr. Huang *et al.* developed electrospun nanoporous carbon nanofibers decorated with Ag–Pt bimetallic NPs.[50] Similarly, metal oxide-NPs-doped phthalocyanine and functionalized multi-walled carbon nanotubes decorated on a glassy carbon electrode have been applied for the detection of DA by Mphuthi *et al.* However, the major disadvantages of these works are their complexity and limitations with respect to other applications.[51] Further, previous works discuss the detection of DA only in biological and environmental samples. However, this investigation discusses the modulation of DA by Tyr and Tyr-rich food intake. To understand the physiological effects of Tyr on the neurotransmitter DA, this is an effort to develop an effective platform to study the effect of Tyr with high sensitivity and specificity. With the significant advancement of optical probes, new possibilities can open up for studying the effect of Tyr on the metabolism of DA. The core focus of this work is to develop a sensor to analyse DA with respect to Tyr intake by monitoring the spectral changes. This work addresses the key issues related to the DA levels with the help of Tyr in a holistic and sustainable way.

4. Conclusion

In summary, the binding interaction of the catecholamine neurotransmitter DA with Au@Ag NPs was successfully studied using various spectroscopic techniques. The interaction of DA with the NPs system was verified by the UV-visible and FTIR analyses. The appearance of the characteristic plasmonic peak at 280 nm confirms the notable interaction of DA with Au@Ag NPs in contrast to the monometallic AuNPs and AgNPs. The major modes of interaction are van der Waals interaction and hydrogen bonding, as demonstrated by the thermodynamic parameters. The increase in binding constant with an increase in temperature emphasises the strong bonding between DA and Au@Ag NPs possibly in a ground–state complex. The as-obtained DA-interacted Au@Ag NPs system was applied to study and analyse the effect of Tyr-rich food as a dietary precursor of DA in the body. The results indicate that Tyr-rich food consumption may counteract depletion in DA function and cognitive performance. This study supports the effectiveness of Tyr supplementation as a beneficial treatment for improving behavioural performance, clinical disorders, and DA synthesis and function. Furthermore, Tyr along with DA can act as a promising cognition and mood enhancer. Thus, this one-of-a-kind analytical study proposes a strategy to enhance DA levels through Tyr based on the findings obtained using Au@Ag NPs as a sensing platform.

Author contributions

Angel Minj: writing – original draft, methodology, software, validation, investigation, visualization. Sushama Sahu: writing review & editing, methodology, software, visualization, validation and investigation. Lavkesh Kumar Singh Tanwar: software, validation, investigation. Kallol K. Ghosh: conceptualization, supervision, project administration, funding acquisition. writing – review & editing, project administration.

Conflicts of interest

There are no conflicts to declare.

Acknowledgements

The authors are grateful to the National Center for Natural Resources, Pt. Ravishankar Shukla University, Raipur (C. G.) for providing the FTIR facility. Also, to the Sophisticated Analytical Instrument Facility (SAIF), at the Indian Institute of Technology, Bombay (MH) for HR-TEM analysis. The authors wish to thank Advanced Material Research Center, Indian Institute of Technology Mandi for the XPS analysis.

References

1 E. Nam, J. S. Derrick, S. Lee, J. Kang, J. Han, S. J. Lee, S. W. Chung and M. H. Lim, *ACS Chem. Neurosci.*, 2018, **9**, 2655–2666.
2 A. P. F. Chen, L. Chen, T. A. Kim and Q. Xiong, *Biomedicines*, 2021, **9**, 1–29.
3 A. Suzuki, T. A. Ivandini, K. Yoshimi, A. Fujishima, G. Oyama, T. Nakazato, N. Hattori, S. Kitazawa and Y. Einaga, *Anal. Chem.*, 2007, **79**, 8608–8615.
4 A. A. Banday and M. F. Lokhandwala, *Curr. Hypertens. Rep.*, 2008, **10**, 268–275.
5 S. Latif, M. Jahangeer, D. Maknoon Razia, M. Ashiq, A. Ghaffar, M. Akram, A. El Allam, A. Bouyahya, L. Garipova, M. Ali Shariati, M. Thiruvengadam and M. Azam Ansari, *Clin. Chim. Acta*, 2021, **522**, 114–126.
6 R. A. Wise and C. J. Jordan, *J. Biomed. Sci.*, 2021, **28**, 1–9.
7 H. C. Lou, *Acta Paediatr.*, 1994, **83**, 86–88.
8 P. B. Foley, *J. Neural Transm.*, 2019, **126**, 473–479.
9 X. Tan, W. Song, X. Chen, L. Liu and J. Wu, *Appl. Microbiol. Biotechnol.*, 2020, **104**, 9907–9920.
10 Z. Li, T. Hong, G. Shen, Y. Gu, Y. Guo and J. Han, *Nutrients*, 2022, **14**(3887), 1–34.
11 A. Slominski, M. A. Zmijewski and J. Pawelek, *Pigm. Cell Melanoma Res.*, 2011, **25**, 14–27.
12 B. J. Jongkees, B. Hommel, S. Kühn and L. S. Colzato, *J. Psychiatr. Res.*, 2015, **70**, 50–57.
13 M. Jefri, S. Bell, H. Peng, N. Hettige, G. Maussion, V. Soubannier, H. Wu, H. Silveira, J.-F. Theroux, L. Moquin, X. Zhang, Z. Aouabed, J. Krishnan, L. A. O'Leary, L. Antonyan, Y. Zhang, V. McCarty, N. Mechawar, A. Gratton, A. Schuppert, T. M. Durcan, E. A. Fon and C. Ernst, *Stem Cells Transl. Med.*, 2020, **9**, 697–712.
14 M. J. Kim, Y. Moon, J. C. Tou, B. Mou and N. L. Waterland, *J. Food Compos. Anal.*, 2016, **49**, 19–34.
15 A. Hase, S. E. Jung and M. aan het Rot, *Pharmacol., Biochem. Behav.*, 2015, **133**, 1–6.
16 W. R. Algar, T. Albrecht, K. Faulds and J.-J. Zhu, *Analyst*, 2022, **147**, 765–766.
17 S. Balasurya, P. Ahmad, A. M. Thomas, L. L. Raju, A. Das and S. Sudheer Khan, *Opt. Commun.*, 2020, **464**, 125512–125520.
18 H. K. Daima, P. R. Selvakannan, A. E. Kandjani, R. Shukla, S. K. Bhargava and V. Bansal, *Nanoscale*, 2014, **6**, 758–765.
19 R. Pahuja, K. Seth, A. Shukla, R. K. Shukla, P. Bhatnagar, L. K. Chauhan, P. N. Saxena, J. Arun, B. P. Chaudhari, D. K. Patel, S. P. Singh, R. Shukla, V. K. Khanna, P. Kumar, R. K. Chaturvedi and K. C. Gupta, *ACS Nano*, 2015, **9**, 4850–4871.
20 L. Schoonen and J. C. van Hest, *Nanoscale*, 2014, **6**, 7124–7141.
21 P. Tsai, K. Chuang, C. Yang, H. Lee and F. Lu, *J. Alloys Compd.*, 2019, **785**, 191–195.
22 Z. Niu and Y. Li, *Chem. Mater.*, 2013, **26**, 72–83.
23 P. Srinoi, Y. Chen, V. Vittur, M. Marquez and T. Lee, *Appl. Sci.*, 2018, **8**, 1106–11038.
24 B. Xia, F. He and L. Li, *Langmuir*, 2013, **29**, 4901–4907.
25 M. Daniel and D. Astruc, *Chem. Rev.*, 2004, **104**, 293–346.
26 J. B. Essner, K. Pokpas, J. A. Canon, N. Jahed, E. I. Iwuoha and G. A. Baker, *J. Phys. Chem. C*, 2018, **122**, 5105–5118.
27 L. Panariello, S. Damilos, H. du Toit, G. Wu, A. N. Radhakrishnan, I. P. Parkin and A. Gavriilidis, *React. Chem. Eng.*, 2020, **5**, 663–676.
28 M. T. Alula, L. Karamchand, N. R. Hendricks and J. M. Blackburn, *Anal. Chim. Acta*, 2018, **1007**, 40–49.
29 S. Sahu, S. Sharma, T. Kant, K. Shrivas and K. K. Ghosh, *Spectrochim. Acta, Part A*, 2021, **246**, 118961–118991.
30 S. Sahu, S. Sharma and K. K. Ghosh, *New J. Chem.*, 2020, **44**, 15010–15017.
31 H. Zhang, J. Okuni and N. Toshima, *J. Colloid Interface Sci.*, 2011, **354**, 131–138.
32 R. Kurrey, M. K. Deb, K. Shrivas, J. Nirmalkar, B. K. Sen, M. Mahilang and V. K. Jain, *RSC Adv.*, 2020, **10**, 40428–40441.
33 A. Saha, B. R. Khalkho and M. K. Deb, *RSC Adv.*, 2021, **11**, 20380–20390.
34 A. Thakur, S. Ranote, D. Kumar, K. K. Bhardwaj, R. Gupta and G. S. Chauhan, *ACS Omega*, 2018, **3**, 7925–7933.
35 C. V. Durgadas, C. P. Sharma and K. Sreenivasan, *Nanoscale*, 2011, **3**, 4780–4787.
36 P. Wagener, A. Schwenke and S. Barcikowski, *Langmuir*, 2012, **28**, 6132–6140.
37 J. W. Park and J. S. Shumaker-Parry, *J. Am. Chem. Soc.*, 2014, **136**, 1907–1921.
38 S. Nath, S. K. Ghosh, S. Kundu, S. Praharaj, S. Panigrahi and T. Pal, *J. Nanopart. Res.*, 2006, **8**, 111–116.
39 K. Shrivas, S. Sahu, G. K. Patra, N. K. Jaiswal and R. Shankar, *Anal. Methods*, 2016, **8**, 2088–2096.
40 H. Zhang, M. Haba, M. Okumura, T. Akita, S. Hashimoto and N. Toshima, *Langmuir*, 2013, **29**, 10330–10339.
41 L. Vitos, A. V. Ruban, H. L. Skriver and J. Kollár, *Surf. Sci.*, 1998, **411**, 186–202.
42 W. H. Qi and M. P. Wang, *J. Phys. Chem. B*, 2005, **109**, 22078–22079.
43 Y. Li, W. Qi, B. Huang, W. Ji and M. Wang, *J. Phys. Chem. C*, 2013, **117**, 15394–15401.
44 A. Loiseau, V. Asila, G. Boitel-Aullen, M. Lam, M. Salmain and S. Boujday, *Biosensors*, 2019, **9**, 78.
45 Reshma, S. K. Vaishnav, I. Karbhal, M. L. Satnami and K. K. Ghosh, *J. Mol. Liq.*, 2018, **255**, 279–287.

46 S. Sahu, Reshma, S. Sharma, I. Karbhal and K. K. Ghosh, *RSC Adv.*, 2020, **10**, 31400–31410.
47 S. Sahu and K. K. Ghosh, *Anal. Methods*, 2022, **14**, 3323–3334.
48 D. Du, Y. Su, Q. Shang, C. Chen, W. Tang, L. Zhang, H. Ren and W. Liu, *J. Inorg. Biochem.*, 2022, **234**, 111878–111900.
49 Z. Zhou, W. Saw, P. Ho, Z. Zhang, L. Zeng, Y. Chang, A. Sun, D. Ma, H. Wang, L. Zhou, K. Lim and E.-K. Tan, *Cell. Mol. Life Sci.*, 2022, **79**, 1–21.
50 Y. Huang, Y.-E. Miao, S. Ji, W. W. Tjiu and T. Liu, *ACS Appl. Mater. Interfaces*, 2014, **6**, 12449–12456.
51 N. Mphuthi, A. Adekunle, O. Fayemi, L. Olasunkanmi and E. Ebenso, *Sci. Rep.*, 2017, **7**, 1–21.